Layered ferromagnet/superconductor heterostructures: Nonequilibrium quasiparticle dynamics and photodetector applications

D. Pan,[1,2] G. P. Pepe,[3] V. Pagliarulo,[3] C. De Lisio,[3] L. Parlato,[3] M. Khafizov,[1,2] I. Komissarov,[2,4] and Roman Sobolewski[1,2,4]
[1]*Department of Physics and Astronomy, University of Rochester, Rochester, New York 14627-0171, USA*
[2]*Laboratory for Laser Energetics, University of Rochester, Rochester, New York 14623, USA*
[3]*CNR-INFM Coherentia and Dipartimento Scienze Fisiche, Università di Napoli "Federico II," Piazzale Tecchio 80, I-80125 Napoli, Italy*
[4]*Department of Electrical and Computer Engineering, University of Rochester, Rochester, New York 14627-0231, USA*
(Received 19 February 2008; revised manuscript received 18 September 2008; published 5 November 2008)

Time-resolved optical pump-probe and photoimpedance studies of proximized ferromagnet/superconductor nanobilayers are presented. The weak ferromagnetic nature of an ultrathin $Ni_{0.48}Cu_{0.52}$ film makes it possible to observe the dynamics of the nonequilibrium superconductivity in NiCu/Nb hybrids through time-resolved measurements of a near-surface optical reflectivity change, which is generated by femtosecond optical pump pulses and discussed within a nonequilibrium two-temperature electron-heating model. We observed that the NiCu overlay significantly reduced the slow bolometric contribution present in the photoresponse of a pure Nb film, resulting in a strong enhancement of the nonequilibrium kinetic-inductive component of the transient photoimpedance, measured as an ~700-ps-wide voltage waveform generated across an optically excited current-biased NiCu/Nb bilayer microbridge. The sensitive picosecond photoresponse makes our NiCu/Nb heterostructures suitable for "engineered" ultrafast superconducting photodetectors since the photoimpedance signals observed in plain Nb bridges were at least 10 ns long and were due to the light-induced simple-heating effect.

DOI: 10.1103/PhysRevB.78.174503 PACS number(s): 74.40.+k, 74.70.−b, 74.72.−h, 74.45.+c

I. INTRODUCTION

Superconducting devices offer unique performance for fast and ultrasensitive optical detection because of their quantum nature with the low, as compared to typical semiconductors, magnitude of the energy gap Δ, ultrafast Cooper-pair and quasiparticle (QP) dynamics, low noise, and stable cryogenic-operation environment.[1] The small value of Δ, which is typically 3 orders of magnitude lower than that, e.g., in Si, makes it possible to generate an efficient avalanche of excited QPs in a superconducting material, even upon absorption of a single optical photon.[2] The QP multiplication effect enhances resolution in energy-resolving superconducting devices, such as superconducting tunnel junctions,[3] and extends the range of detectable wavelengths into the midinfrared region for, e.g., single-photon counters.[4] Moreover, the energy-relaxation time constants of QPs in thin- and ultrathin-film structures are in the picosecond range for, respectively, high- and low-temperature superconductors, assuring repetition rates in the gigahertz range.[5]

After absorption of an optical photon with the energy $\hbar\omega \gg 2\Delta$, a local nonequilibrium distribution of both QPs and phonons is created in a superconducting thin film. The hot electrons relax down in energy through the electron-electron (e-e) and electron-phonon (e-ph) interactions, resulting in a temperature T_e increase in the electron subsystem. Spatially, this thermalization phase is characterized by formation and growth of a hotspot, a local nonsuperconducting (or superconductivity-suppressed) region inside a superconducting material.[6] If the superconducting sample is a nanowire-type structure consisting, e.g., of an ultrathin ($d_S \sim \xi_S \sim$ few nanometers) and submicrometer-wide (~100-nm-wide) stripe, even a hotspot generated by absorption of a single photon can produce a measurable impact, due to the generation of phase-slip centers and the subsequent appearance of a voltage signal across the current-biased stripe.[2] The hotspot formation process competes, of course, with the cooling process as QPs diffuse out of the hotspot and recombine into Cooper pairs. Thus, after a time, depending on both the diffusion rate and the QP relaxation dynamics, the hotspot heals itself, leading to the restoration of the superconducting path along the nanostripe.

If an optically irradiated superconducting sample is of a micrometer size or larger and the flux of photons is insufficient to generate enough overlapping hotspots to completely ruin the superconductivity, a different effect occurs, namely, the kinetic-inductive photoresponse, which is based on the inertialike inductive response of a superconducting condensate.[7] Under optical irradiation, the kinetic inductance L_{kin} of a superconducting sample is determined by the nonequilibrium energy distribution function of QPs $f(\varepsilon)$ and by the value of Δ and is given as

$$\frac{1}{L_{\mathrm{kin}}} = \frac{\sigma_n}{\hbar}\int_{\Delta-\hbar\Omega}^{\Delta} d\varepsilon[1-2f(\varepsilon - \hbar\Omega)]\frac{\varepsilon(\varepsilon+\hbar\Omega)+\Delta^2}{\sqrt{(\Delta^2-\varepsilon^2)}\sqrt{(\varepsilon+\hbar\Omega)^2-\Delta^2}}, \quad (1)$$

where σ_n is the normal-state conductivity and the integral is taken over energies $\hbar\Omega$ close to Δ.[8]

Time evolution of both the phonon and QP distribution functions can be described by a system of coupled microscopic kinetic equations.[9] At $T \leqslant T_c$, where T_c is the superconductor critical temperature, and under weak perturbations, we can assume that the electron and phonon dynamics

are described in terms of the energy distributions and assign two different temperatures, T_e and T_{ph}, which characterize their relevant subsystems. By neglecting any heat diffusion after the energy absorption, the nonequilibrium state can, therefore, be described by a system of two coupled differential time-dependent energy-balance equations commonly referred as the two-temperature (2T) model,[10]

$$C_e \frac{dT_e}{dt} = -\frac{C_e}{\tau_{e\text{-ph}}}(T_e - T_{\mathrm{ph}}) + S(t),$$

$$C_{\mathrm{ph}} \frac{dT_{\mathrm{ph}}}{dt} = -\frac{C_{\mathrm{ph}}}{\tau_{\mathrm{ph}\text{-}e}}(T_{\mathrm{ph}} - T_e) - \frac{C_{\mathrm{ph}}}{\tau_{\mathrm{esc}}}(T_{\mathrm{ph}} - T_0), \tag{2}$$

where $S(t)$ represents the laser source, C_e and C_{ph} are the electron- and phonon-heat capacities, respectively, $\tau_{e\text{-ph}}$ and $\tau_{\mathrm{ph}\text{-}e}$ are the e-ph and ph-e relaxation times, respectively, τ_{esc} is the characteristic time for phonons to escape out to the substrate or decay anharmonically, and T_0 is the bath temperature. In superconducting metals, T_e evolves on a time scale of the order of a few picoseconds, while T_{ph} changes typically on a nanosecond scale.

At low-excitation fluencies and/or near T_c, the temperature dependences of C_e and C_{ph} can be neglected and the simple energy balance,

$$\frac{C_e}{\tau_{e\text{-ph}}} = \frac{C_{\mathrm{ph}}}{\tau_{\mathrm{ph}\text{-}e}}, \tag{3}$$

is preserved.[11]

Solution of the 2T equations gives direct information about the involved nonequilibrium QP and phonon dynamics, such as the $\tau_{e\text{-ph}}$ value. Simultaneously, the T_e time evolution can be used to calculate L_{kin} through the following equation:[12]

$$L_{\mathrm{kin}} = \frac{1}{\varepsilon_0 \omega_p^2} \frac{1}{1 - \left(\frac{T_e}{T_c}\right)^2} \frac{l}{wd}, \tag{4}$$

where ω_p is the plasma frequency of the superconductor and l, w, and d are the length, width, and thickness of a microbridge-type superconducting sample, respectively. Accordingly, the change of L_{kin} can be quite large and lead to a measurable voltage transient across the bridge given by

$$V_{\mathrm{kin}} = I_b(dL_{\mathrm{kin}}/dt), \tag{5}$$

where I_b is the sample bias current.

The choice of material is crucial since various superconductors have a drastically different kinetic response in terms of the $\tau_{e\text{-ph}}$ scattering, C_e/C_{ph} ratio, and τ_{esc}. NbN and $YBa_2Cu_3O_{7-x}$ (YBCO) have been demonstrated to be rather optimal choices as superconducting materials for bridge-type superconducting photodetectors as they are characterized by the overall picosecond photoresponse.[13,14]

Besides simple metals, heterogeneous bilayer structures formed by a superconductor (S) and a normal (N) metal in a good electrical contact represent a new approach in superconducting devices since they can be optimized toward achieving the ultrafast carrier dynamics.[15] According to the physics of the proximity effect, near the bilayer S/N interface, both materials influence each other on a spatial scale of their coherence lengths (ξ_S and ξ_N, respectively). In well-investigated proximized bilayers, such as Al/Nb, Ta/Nb, or Al/Ta, the S/N interface is highly transparent and ξ_S and ξ_N are always much larger than the material optical penetration depth α [typically below 50 nm at the visible-light (400–900 nm) wavelength range]. Thus, for optical studies, the ultrathin N layer with the thickness comparable to α represents too-small N metal perturbation in order to quantitatively measure any proximity-related effects. On the other hand, optically thick N overlayers simply attenuate too much light, preventing any optical studies of the buried underneath interface. As a result N/S bilayers are not attractive subjects for photoresponse experiments nor photodetector applications.

In the view of the above, weak-ferromagnet/superconductor (F/S) proximity bilayers are unique in this context since ξ_F is $\leqslant 10$ nm due to the presence of the magnetic exchange energy. Thus, in F/S heterostructures, the superconducting properties vary significantly over the distance comparable to the visible light α and they are "natural" choice for optical characterization.[16] We want to stress that strong ferromagnets, such as pure Fe, Ni, or Permalloy, are often implemented in F/S heterostructures, but they are far less suitable for the optical experimentation as the their case $\xi_F \sim 1$ nm is much smaller than α.[17] Finally, we expect that recently developed F/S heterostructures, based on YBCO and ferromagnetic manganites, such as La-Sr-Mn-O (LSMO),[18] which represent a novel combination of oxide materials, should be well suited for optical characterization and photodetector applications. These epitaxially grown F/S bilayers combine the ultrafast QP photoresponse of YBCO with the large electromagnetic field penetration depth and high spin polarization. La-Ca-Mn-O/YBCO oxide superlattices[19] show a long-range interplay between ferromagnetism and superconductivity and a clear indication of the F/S proximity effect. Very recently, we have observed that the photoresponse of the LSMO/YBCO bilayer exhibits a very pronounced shortening of the relaxation time in recovering into the equilibrium state.[20] Apparently, the proximity effect makes the manganite layer an effective trapping layer for QPs which diffuse from YBCO, but more research is needed to, e.g., fully understand the role of an additional relaxation channel related to the spin interactions due to the almost perfect half-metal nature of LSMO and the superconducting state of YBCO.

We report here our time-resolved all-optical (pump-probe) photoresponse and electronic photoimpedance studies performed on fully proximized NiCu/Nb superconducting F/S microbridges and compare them with the results obtained in the case of a pure-Nb superconductor. Upon 100-fs-wide optical pulse excitation, our heterostructures show a significantly higher transient T_e increase, which leads to a subnanosecond-in-duration (limited by the bandwidth of our electronics) kinetic-inductance photoresponse, which is absent in the pure Nb bridges studied under the same experimental conditions. The use of proximized bilayers can be further extended to other superconducting materials, leading to "custom-designed" superconductors with refined optical

TABLE I. $Ni_{0.48}Cu_{0.52}$/Nb and pure Nb sample specifications.

	Sample A	Sample B
Thickness of Nb layer (nm)	100	70
Thickness of $Ni_{0.52}Cu_{0.48}$ layer (nm)	0	21
Width of the bridge (μm)	10	5
Length of the bridge (μm)	100	50

performances in terms of the photodetection response and sensitivity reaching the single-photon limit. In Sec. II, we give a brief overview of our fabrication process of NiCu/Nb bilayers and microbridges and our measurement procedures. Section III presents our experimental results and discusses them in the framework of the nonequilibrium 2T model and the kinetic-inductive and resistive photoimpedance responses. Finally, our conclusions and future prospects of NiCu/Nb nanostructures as efficient photon detectors and counters are discussed in Sec. IV.

II. EXPERIMENTAL PROCEDURES

Thin films of Nb and $Ni_{0.48}Cu_{0.52}$ alloy were deposited by using two dedicated dc magnetron-sputtering systems. Our fabrication procedure was described in Ref. 21; briefly, 70-nm-thick base Nb layers were sputtered at a base pressure of 1×10^{-7} Torr on chemically cleaned Corning glass substrates. The sputtering power density and deposition rate were 10 W/cm^2 and 2.2 nm/s, respectively. Next, the Nb samples were inserted into a NiCu deposition system, where their surface was first precleaned for 30 s using ion-beam etching at a rate of about 0.2 nm/s. Afterward $Ni_{0.48}Cu_{0.52}$ films were sputtered at a rate of 1.5 nm/s using a power density of 10 W/cm^2. The NiCu thickness of the sample used for photodetection experiments was 21 nm. The energy-dispersive x-ray spectroscopy analysis confirmed that the composition of the deposited alloy was very close to the source target.[22] Low-temperature magnetization tests for as-deposited NiCu films showed a Curie temperature of $\leqslant$30 K and a spontaneous moment per atom $\mu_0=0.06\mu_B$/atom at $T=4.2$ K; both values are typical for a weak ferromagnetism.[16]

Our test samples were "H-type" structures, patterned from a 100-nm-thick Nb film (sample A) and NiCu(21-nm)/Nb(70-nm) bilayers (sample B) and consisted of microbridges placed between the signal line and the ground line of a 50 Ω coplanar stripline (CSL). The main specifications and microbridge dimensions are summarized in Table I. The samples were mounted on a Cu cold finger, inside of a temperature-controlled liquid-helium optical cryostat operating down to 4 K. The NiCu/Nb superconducting transition, measured by the constant-current method, was $T_c=8.5$ K, which corresponds to the T_c of the bottom (shunting) Nb layer. The actual T_c of the bilayer was estimated to be ~8 K from the temperature dependence of the Josephson critical current in tunnel junctions containing the same bilayer as an electrode.[21]

Figure 1 presents critical current density (J_c) dependences for both samples A (pure Nb) and B (NiCu/Nb) on temperature. We note that contrary to the most recent work of Angrisani Armenio *et al.*,[23] we observe an enhancement of J_c for the F/S bilayer as compared to the pure Nb microbridge. The pinning of vortices in proximized superconducting bilayers represents a quite interesting field of investigation, and different physical mechanisms have been proposed for the explanation of the J_c enhancement observed in F/S structures.[24] Our F layer consists of a weak ferromagnet instead of Permalloy as in Ref. 23; thus, we expect a homogeneous vortex pinning in both films, which should be enhanced for NiCu/Nb bridges due to the presence of the NiCu overlayer. The latter is clearly visible in Fig. 1 (inset), which presents the current-voltage (I-V) characteristics of both microbridges in a semilogarithmic scale, measured at 8 K. Both curves exhibit behavior that is typical of a long superconducting constriction with a wide jump to the fully resistive state, but in the case of the Nb bridge we can clearly identify a well-developed flux-flow region at low voltages, which is essentially missing in the NiCu/Nb sample, apparently due to a much stronger pinning. Detailed experiments are in progress in order to understand the role of ferromagnetic artificial pinning centers, apparently, due to Ni clusters near the F/S interface, as well as the potential magnetic anisotropy of the F layer.[25] Nevertheless, this aspect of the F/S research is well behind the aim of this paper.

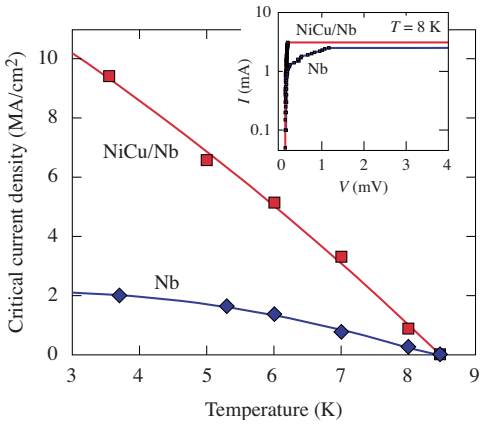

FIG. 1. (Color online) Critical current density dependence on temperature for our NiCu/Nb and Nb microbridges. The inset shows the actual I-V characteristics in the semilogarithmic scale of both samples taken at 8 K.

Our bilayer samples were first optically characterized by performing time-resolved normalized reflectivity change $\Delta R/R$ measurements. Femtosecond pump-probe spectroscopy experiments were performed in reflection mode in a system earlier presented in Ref. 22 using a commercial MIRA900F mode-locked Ti:sapphire laser, which produced a train of 100-fs-long pulses at a wavelength of 810 nm and a repetition rate of 76 MHz. The main train was split into the pump and probe beams, which were focused onto the sample down to $<$30 μm in diameter and cross polarized to eliminate coherent artifacts caused by their direct interference. The pump average incident power was ~5 mW and the pump-probe energy ratio was 10:1. Such conditions ensured the absence of any trivial thermal effects, such as significant pump heating, while ensuring a good signal-to-noise ratio.

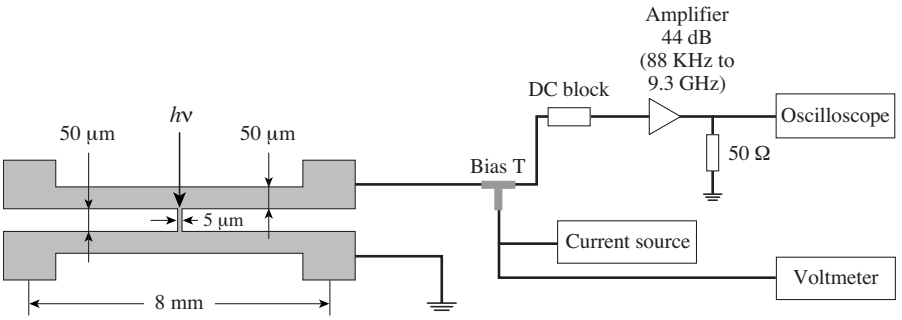

FIG. 2. Time-resolved photoimpedance experiment setup.

For time-resolved photoimpedance experiments, which mimic photodetector operation, we used the experimental setup shown schematically in Fig. 2. The CSL with the microbridge was connected to the dc bias and rf output circuitry through a broadband cryogenic bias tee, and the whole arrangement was placed on a Cu cold plate inside our temperature-controlled continuous-flow helium cryostat. Outside the Dewar, the device output was fed into a low-noise broadband amplifier (bandwidth: 88 MHz to 9.3 GHz) characterized by a 44 dB gain. As a light source, we used in this case a portable mode-locked IMRA fiber laser, generating 130-fs-wide pulses at a wavelength of 780 nm and a repetition rate of 50 MHz. The intensity of the incident radiation was attenuated in a very wide range using banks of neutral-density filters. During the experiments, our samples were uniformly illuminated with a fluence per pulse in the $0.7 < J_{in} < 10$ fJ/μm^2 range at the bridge plane.

III. EXPERIMENTAL RESULTS AND DISCUSSION

Figure 3 presents the $\Delta R/R$ signals (open dots) as a function of time for the NiCu/Nb [sample B, Fig. 3(a)] and Nb [sample A; Fig. 3(b)] films, maintained at $T < T_c$. We note that the NiCu/Nb transient exhibits a very sharp, approximately 150 fs in duration, pump-pulse-width limited initial peak, followed by an initial subpicosecond decay and a slowly decaying plateau. The Nb $\Delta R/R$ signal exhibits the same fast rise but is dominated by the plateau behavior. As we have already demonstrated in Ref. 22 (in particular, see the data related to samples A and E, as their morphologies are the closest to the samples studied in this work) within the measured time window of 20 ps, the $\Delta R/R$ transients (no matter if measured above or below T_c) decay exponentially with the two characteristic relaxation times: τ_{fast} and τ_{slow}. The first one is subpicosecond and was identified in Ref. 22 as the e-ph relaxation time, and its temperature dependence was used to evaluate the e-ph coupling constant $g_{e\text{-ph}}$ in our proximized F/S heterostructures by calculating the density of states functions for the tested bilayers, while τ_{slow} (a few picoseconds long) was directly linked to the near-band-gap interaction of QPs with acoustic phonons. The $\Delta R/R$ relaxation following τ_{slow} (essentially a plateau within our time window in Fig. 3) corresponds to the $T_{ph}(t)$ dynamics, which very strongly depends on the thickness of the NiCu overlayer, and the film/substrate acoustic transparency [τ_{esc} in Eq. (2)].

Since in this work we are mostly interested in the $T_e(t)$ time evolution after the photon absorption, which is needed to estimate $L_{kin}(t)$ [Eq. (4)] and, eventually, predict the temporal shape [Eq. (5)] of photoimpedance signals measured in a setup presented in Fig. 2, we decided to focus here on the e-ph relaxation process and numerically solved the 2T model [Eq. (2)] based on the energy balance relation [Eq. (3)]. In our calculations, we assumed that the quasiparticles were characterized by the Fermi distribution function, as our pump pulse of 100 fs is much longer than the few-femtosecond-long e-e relaxation time. We also took into account that our 30-μm-diameter laser beam spot size was much greater than $\alpha \approx 50$ nm, as well as the electron penetration depth (tens of hundreds of nanometers), so the one-dimensional model accurately represented our experimental situation. Finally, we neglected the heat diffusion out of the optical excitation region since our experimental window was much shorter than τ_{esc}, and we assumed a Gaussian profile of the incident laser pump pulse.

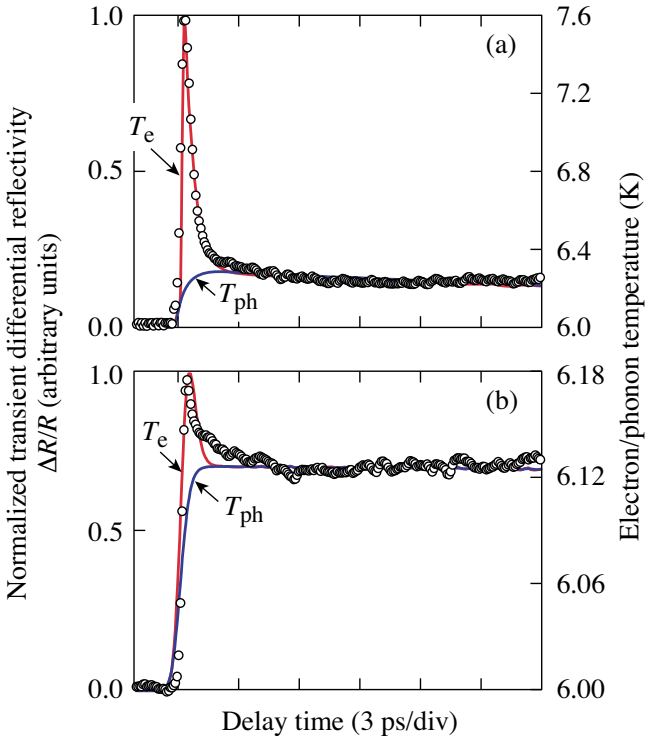

FIG. 3. (Color online) Normalized reflectivity change as a function of time (open circles), measured at 6 K for (a) NiCu/Nb and (b) Nb samples. The solid lines are the electron and phonon temperature transients, respectively, numerically evaluated for our films using the 2T model [see Eq. (2)]. The right y axes show the actual increase in the electron/phonon temperature.

The resulting $T_e(t)$ and $T_{ph}(t)$ time evolutions are shown as solid lines in Figs. 3(a) and 3(b), and we note that especially in the case of the NiCu/Nb sample [Fig. 3(a)] the single-exponential $T_e(t)$ transient, represented by the $\tau_{e\text{-ph}}$ decay, fits the $\Delta R/R$ signal very satisfactorily, emphasizing that under the conditions of our experiment, $\Delta R/R$ is directly related to the T_e dynamics, which, in turn, is governed by the nonequilibrium e-ph relaxation. The best fits presented in Fig. 3 were obtained for the $C_{ph}/C_e=6.4$ and $C_{ph}/C_e=2.7$ values, and $\tau_{e\text{-ph}}$ equal to 0.46 and 0.21 ps (the fits to the early T_e relaxation parts of $\Delta R/R$) for our NiCu/Nb and Nb samples, respectively. Extracting the accurate values of τ_{esc} was a difficult task due the short experimental time window of our $\Delta R/R$ transients. Thus, we could only get rough estimates and, accordingly, $T_{ph}(t)$ fits in Fig. 3 were obtained with τ_{esc}'s on the order of ~300 ps and approximately 10–20 ns for NiCu/Nb and Nb, respectively. The maximum ΔT_e change reached in NiCu/Nb and Nb samples during the laser pumping was 1.6 and 0.18 K, respectively. On the other hand, the peak amplitude of the $T_{ph}(t)$ evolution for both samples was almost negligibly small since their ΔT_{ph}'s remained in the 2%–3% range of the bath temperature.

Our $\tau_{e\text{-ph}}$ values listed above are close to the corresponding experimental τ_{fast} parameters obtained in Ref. 22. Thus, we used them together with the experimental C_{ph}/C_e fit ratios and the $g_{e\text{-ph}}$ values from Ref. 22 and Eq. (3) in order to calculate the actual values of C_e, C_{ph}, and $\tau_{ph\text{-}e}$ for our samples. The resulting values of C_e, C_{ph}, and $\tau_{ph\text{-}e}$ are 1.54 mJ/(K cm^3), 9.86 mJ/(K cm^3), and 2.9 ps and 3.48 mJ/(K cm^3), 9.4 mJ/(K cm^3), and 0.57 ps for NiCu/Nb and Nb, respectively. We note that both sets of specific heat values are different than those published in Ref. 22, but we must stress that previously we deduced the C_e values from the density-of-states (DoS) calculations numerically evaluated at the free surface of the top F layer without taking into account the actual spatial dependence of the DoS inside the two films and close to the interface, while the estimation of the C_{ph} for NiCu/Nb was based on the $C_{ph}=\beta T^3$ law with the coefficient β obtained by averaging the β(Nb) and β(NiCu) values with the bilayer thicknesses normalized to α's as weights.[26] Our presented here set of parameters is not only based on the experimental data but is much more realistic since in the case of NiCu/Nb the condition $C_e/C_{ph} \ll 1$ must be fulfilled in order to observe the transient photoresponse dominated by the electronic subsystem ($\tau_{e\text{-ph}}/\tau_{ph\text{-}e} \ll 1$) with a low value of the phonon plateau. At the same time, $g_{e\text{-ph}}$ depends only on the averaged specific heat capacity and is much less sensitive to the C_{ph}/C_e ratio.

Comparing the (C_e and T_e) and (C_{ph} and T_{ph}) sets for the NiCu/Nb and Nb samples, we observe that the presence of the NiCu film only marginally affects the phonon subsystem with the only exception of the much shorter estimated τ_{esc} value. Such behavior is expected as the bulk of the NiCu/Nb sample consists of the Nb film. Although in both cases we have the same Nb-glass interface, the F overlayer acts as parallel heat sink, providing efficient anharmonic decay for the acoustic phonons and significantly reducing τ_{esc}. However, the "phonon sink" is not the only role of the NiCu film in NiCu/Nb bilayers; a significant decrease in C_e and approximately ten times increase in the T_e peak value demonstrate that the electron subsystem cooling ($\tau_{e\text{-ph}}/\tau_{ph\text{-}e} \ll 1$) is the dominant mechanism in the QP nonequilibrium relaxation in NiCu/Nb bilayers. Nevertheless, it is important to stress that it is difficult to properly derive the DoS for the actual NiCu-Nb interface and the one presented in Ref. 22 is an apparent oversimplification due to the large atomic segregation of Ni atoms observed within the F/S interface volume of our samples (see Fig. 1 in Ref. 22).

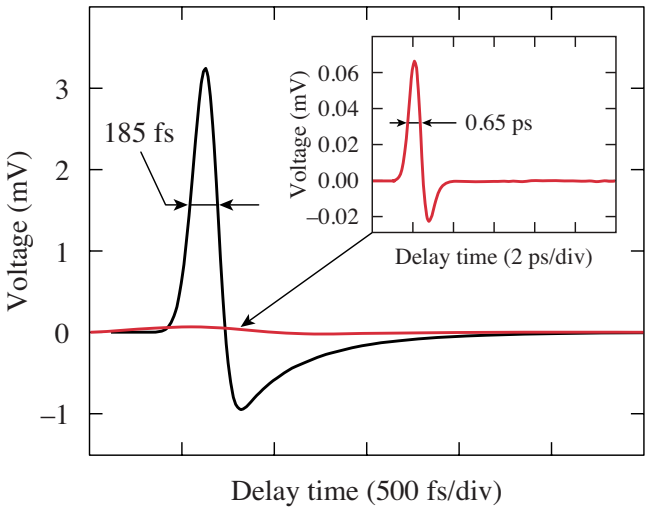

FIG. 4. (Color online) Numerical simulations of V_{kin} as a function of time, obtained using the 2T model solutions plotted in Fig. 3 and Eqs. (4) and (5) for our NiCu/Nb (large oscillatory curve) and Nb (inset) samples. The bias current in both cases was $I_b/I_c=0.43$.

The sharp peak in the $T_e(t)$ dependence for NiCu/Nb indicates that, according to Eq. (4), the microbridge made out of such bilayer should have a much stronger kinetic-inductive photoresponse compared to the one made out of pure Nb. The latter observation is directly supported by the $V_{kin}(t)$ photoimpedance transient simulations presented in Fig. 4. The pronounced oscillatory transient with the full width at half maximum (FWHM) of the main pulse equal to 185 fs corresponds to the NiCu/Nb microbridge, while essentially negligible, in the same voltage scale, response with FWHM=650 fs (see inset in Fig. 4) is that of the Nb bridge. In order to make this comparison meaningful, we assumed that the bridges had the same geometrical parameters and the ω_p values, and we inserted into Eq. (4) the digitized numerical dependences of $T_e(t)$ taken directly from the fits presented in Fig. 3. The bias for both bridges [see Eq. (5)] was also taken to be the same and equal to $0.43I_c$.

Our experimental tests performed on the sample types of the geometry listed in Table I confirmed the predictions that could be drawn based on Fig. 4; namely, we were unable to measure any kinetic-inductive signal in the case of the pure Nb bridge. On the other hand, the NiCu/Nb-bridge transient, while relatively weak, could be clearly resolved and is shown in Fig. 5. The wave form was measured at $T_0=6.0$ K for a NiCu(21 nm)/Nb(70 nm) microbridge, illuminated with 100 fs optical pulses of ~7 μW of the incident average power, and biased with $I_b/I_c=0.43$. Despite a relatively large level of the noise of the presented transient, its oscillatory nature (positive main pulse followed by a nega-

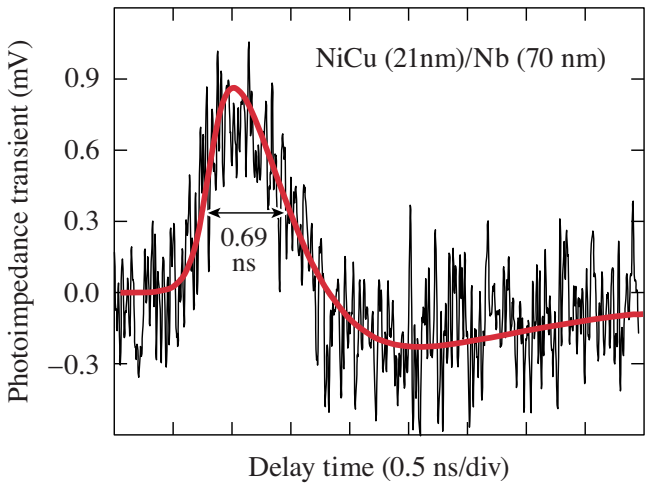

FIG. 5. (Color online) Experimental photoresponse transient of a NiCu/Nb microbridge, acquired at 6 K with I_b=4.5 mA (I_b/I_c =0.43). The solid line is the fit based on the kinetic-inductive model (see Fig. 4), numerically stretched in order to account for the limited bandwidth of our output amplifier.

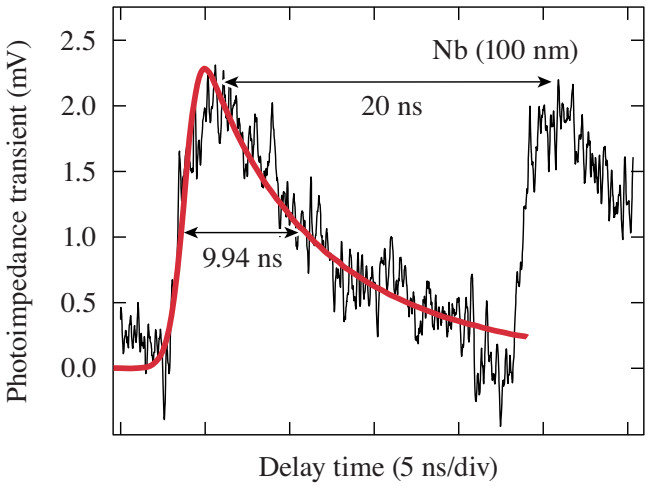

FIG. 6. (Color online) Experimental photoresponse transient of a pure Nb microbridge, acquired at 7 K with I_b/I_c=0.43. The solid line is the fit based on the simple-resistive model [see Eq. (6)]. The incident optical pulse repetition time was 20 ns.

tive component), typical for the superconductive L_{kin} response shown in Fig. 4, can be clearly observed. The thermal contribution was negligible as under our experimental conditions; ΔT_{ph} was negligible for NiCu/Nb [see our earlier discussion following Fig. 3(a)], and we could easily fit the experimental waveform by the simple $V_{\mathrm{kin}}(t)$ expression (thick solid line in Fig. 5) obtained in the same way as the NiCu/Nb transient shown in Fig. 4. The measured FWHM =690 ps is the electronics-limited value, as we numerically stretched the fit by including a high-bandpass filter, corresponding to the upper limit (9.3 GHz) of the bandwidth of our amplifier.

The $V_{\mathrm{kin}}(t)$ fit in Fig. 5 allowed us to estimate the maximum L_{kin} value of ~50 nH for our NiCu/Nb microbridge. In a proximized bilayer, the relation between L_{kin} and the magnetic penetration depth λ is not obvious since any estimation needs to take into account the spatial dependence of the superconducting order parameter. Nevertheless, if we roughly assume that $L_{\mathrm{kin}} \approx (\mu_0 \lambda^2 l)/(wd)$, we get $\lambda \approx 1$ μm at the reduced temperature of our experiment. The obtained λ is much larger than $\leqslant$100 nm typically quoted for pure Nb but, considering the weak ferromagnetic nature of the NiCu overlayer, we find it to be quite reasonable.[27]

In the case of our pure Nb bridges, we could obtain a photoresponse signal only by significantly increasing the incident optical power and/or maintaining the sample at a temperature very close to T_c. Figure 6 presents a photoresponse wave form measured for our sample A biased with I_b/I_c =0.43, the same as in the case of the sample B in Fig. 5 but illuminated with 225 μW of optical power and maintained at 7 K. The over-30-times increase in the optical excitation resulted is a large and relatively slow (FWHM ~10 ns) transient, which, in this case, could be interpreted as simple (Joule-type) optical heating. The incident photons not only broke all the Cooper pairs in the superconductor but also substantially heated up the entire bridge, leading to a temporary increase in the sample temperature above T_c. The thick solid line in Fig. 6 was obtained by using a simple resistive voltage response,

$$V_r(t) = I_b \frac{dR(T)}{dT} \Delta T_{\mathrm{ph}}(t), \tag{6}$$

where $dR(T)/dT$ is the temperature derivative of the experimentally measured resistance versus the temperature curve and $\Delta T_{\mathrm{ph}}(t)$ is the increase in T_{ph} of our system obtained from Eq. (2) [see Fig. 3(b)] with τ_{esc} fitted to the transient photoresponse dependence presented in Fig. 6. We note that $\tau_{\mathrm{esc}} \approx 18$ ns, in very good agreement with our earlier prediction.

IV. CONCLUSIONS

We have reported our time-resolved photoresponse and photoimpedance measurements of superconducting microbridges fabricated from either pure Nb or a proximized NiCu/Nb bilayer. Our experiments demonstrate that the presence of a weakly magnetic NiCu layer on top of the Nb film and the resulting strong proximity effect between the F and S nanolayers significantly modifies the QP dynamics of fully proximized bilayers, as compared to the pristine Nb bridges. In NiCu/Nb bilayers, the bolometric effect has been minimized by the strong enhancement of the $T_e(t)$ dependence, corresponding to the decrease in C_e and decrease in the $\tau_{e\text{-ph}}/\tau_{\text{ph-}e}$ ratio, as compared to pure Nb samples. As a result, we measured an ultrafast kinetic-inductive photoimpedance signal in the case of a current-biased NiCu/Nb microbridge, while in the pure Nb bridges we could observe only a slow nanosecond-in-duration bolometric photoresponse. The former shows that the NiCu/Nb microbridges much better in terms of both the photoresponse signal duration and sensitivity. Clearly, the Nb/NiCu structures and F/S bilayers in general should be considered as very promising materials for high-speed optical photodetectors and, possibly, even photon counters.

ACKNOWLEDGMENTS

This work was partially supported by the MIUR COFIN 2007–2009 "Effetti Quantistici in Nano-strutture e Dispositivi Superconduttivi" (Napoli), by the USAFOSR under Grant No. FA9550-06-1-0348, and the NYSTAR grant to the University of Rochester CAT-EIS (Rochester).

[1] A. D. Semenov, G. N. Gol'tsman, and R. Sobolewski, Supercond. Sci. Technol. **15**, R1 (2002).
[2] G. N. Gol'tsman, O. Okunev, G. Chulkova, A. Lipatov, A. Semenov, K. Smirnov, B. Voronov, A. Dzardanov, C. Williams, and R. Sobolewski, Appl. Phys. Lett. **79**, 705 (2001); R. Sobolewski, A. Verevkin, G. N. Gol'tsman, A. Lipatov, and K. Wilsher, IEEE Trans. Appl. Supercond. **13**, 1151 (2003).
[3] J. N. Ullom, P. A. Fisher, and M. Nahum, Appl. Phys. Lett. **73**, 2494 (1998).
[4] G. Gol'tsman, *et al.*, IEEE Trans. Appl. Supercond. **17**, 246 (2007).
[5] A. Barone, M. Ejrnes, E. Esposito, R. Latempa, S. Pagano, L. Parlato, and G. P. Pepe, Phys. Status Solidi C **3**, 3104 (2006).
[6] A. M. Kadin and M. W. Johnson, Appl. Phys. Lett. **69**, 3938 (1996).
[7] N. Bluzer, Phys. Rev. B **44**, 10222 (1991); F. A. Hegmann and J. S. Preston, *ibid.* **48**, 16023 (1993); M. Lindgren, M. Currie, C. Williams, T. Y. Hsiang, P. M. Fauchet, R. Sobolewski, S. H. Moffat, R. A. Hughes, J. S. Preston, and F. A. Hegmann, Appl. Phys. Lett. **74**, 853 (1999).
[8] A. V. Sergeev, V. V. Mitin, and B. S. Karasik, Appl. Phys. Lett. **80**, 817 (2002).
[9] L. P. Gor'kov and E. M. Éliashberg, Sov. Phys. JETP **29**, 698 (1969); I. E. Bulyzhenkov and B. I. Ivlev, *ibid.* **47**, 115 (1978).
[10] M. L. Kaganov, I. M. Lifshitz, and L. V. Tanatarov, Sov. Phys. JETP **4**, 173 (1957).
[11] A. D. Semenov, R. S. Nebosis, Yu. P. Gousev, M. A. Heusinger, and K. F. Renk, Phys. Rev. B **52**, 581 (1995).
[12] C. J. Stevens and D. J. Edwards, Electron. Lett. **37**, 1420 (2001).
[13] K. S. Il'in, M. Lindgren, M. Currie, A. D. Semenov, G. N. Gol'tsman, R. Sobolewski, S. I. Cherednichenko, and E. M. Gershenzon, Appl. Phys. Lett. **76**, 2752 (2000).
[14] C. Williams, Y. Xu, R. Adam, M. Darula, O. Harnack, J. Scherbel, M. Siegel, F. A. Hegmann, and R. Sobolewski, IEEE Trans. Appl. Supercond. **11**, 578 (2001).
[15] A. Barone and G. Paternò, *Physics and Applications of the Josephson Effect* (Wiley, New York, 1982).
[16] A. A. Golubov, M. Y. Kupriyanov, and E. Il'ichev, Rev. Mod. Phys. **76**, 411 (2004).
[17] A. I. Buzdin, Rev. Mod. Phys. **77**, 935 (2005).
[18] See, for example, Z. Sefrioui, D. Arias, V. Peña, J. E. Villegas, M. Varela, P. Prieto, C. León, J. L. Martinez, and J. Santamaria, Phys. Rev. B **67**, 214511 (2003).
[19] V. Pena, Z. Sefrioui, D. Arias, C. Leon, J. L. Martinez, and J. Santamaria, Eur. Phys. J. B **40**, 479 (2004).
[20] G. P. Pepe *et al.* (unpublished).
[21] G. P. Pepe, R. Latempa, L. Parlato, A. Ruotolo, G. Ausiano, G. Peluso, A. Barone, A. A. Golubov, Ya. V. Fominov, and M. Yu. Kupriyanov, Phys. Rev. B **73**, 054506 (2006).
[22] T. Taneda, G. P. Pepe, L. Parlato, A. A. Golubov, and R. Sobolewski, Phys. Rev. B **75**, 174507 (2007).
[23] A. Angrisani Armenio, C. Cirillo, G. Iannone, S. L. Prischepa, and C. Attansio, Phys. Rev. B **76**, 024515 (2007).
[24] See, for example, M. Lange, M. J. Van Bael, V. V. Moshchalkov, and Y. Bruynseraede, Appl. Phys. Lett. **81**, 322 (2002); A. Garcia-Santiago, F. Sánchez, M. Varela, and J. Tejada, Appl. Phys. Lett. **77**, 2900 (2000); X. X. Zhang, G. H. Wen, R. K. Zheng, G. C. Xiong, and G. J. Lian, Europhys. Lett. **56**, 119 (2001); J. M. E. Geers, M. B. S. Hesselberth, J. Aarts, and A. A. Golubov, Phys. Rev. B **64**, 094506 (2001).
[25] L. N. Bulaevskii, E. M. Chudnovsky, and M. P. Maley, Appl. Phys. Lett. **76**, 2594 (2000).
[26] Y. S. Touloukian and E. H. Buyco, *Specific Heat: Metallic Elements and Alloys*, Thermophysical Properties of Matter Vol. 4 (IFI/Plenum, New York, 1970), and references therein.
[27] J. H. Claassen, S. Adrian, and R. J. Soulen, Jr., IEEE Trans. Appl. Supercond. **9**, 4189 (1999).